Evaluation of a preventive therapy in a model of calcified aortic stenosis

Kevin Prigent

UNIVERSITÉ de CAEN NORMANDIE

UFR SANTÉ

FACULTÉ de MÉDECINE

Année 2019/2020

THÈSE POUR L'OBTENTION

DU GRADE DE DOCTEUR EN MÉDECINE

Présentée et soutenue publiquement le : 14 septembre 2020

par

Mr Kevin PRIGENT

Né le 22 avril 1991 à Rennes (*35*)

TITRE DE LA THÈSE :

Évaluation d'une thérapeutique préventive chez un modèle de rétrécissement aortique calcifié.

Président : **Monsieur le Professeur Denis AGOSTINI**

Membres : Monsieur le Professeur Ludovic BERGER

Monsieur le Professeur Farzin ESMAIL-BEYGUI

Monsieur le Docteur Damien LEGALLOIS

Directeur de thèse : ***Pr Alain MANRIQUE***

UNIVERSITÉ DE CAEN · NORMANDIE

UFR SANTÉ - FACULTE DE MEDECINE

Année Universitaire 2019/2020

Doyen
Professeur Emmanuel TOUZÉ

Assesseurs
Professeur Paul MILLIEZ (pédagogie)
Professeur Guy LAUNOY (recherche)
Professeur Sonia DOLLFUS & Professeur Evelyne EMERY (3ème cycle)

Directrice administrative
Madame Sarah CHEMTOB

PROFESSEURS DES UNIVERSITÉS - PRATICIENS HOSPITALIERS

M.	**AGOSTINI Denis**	Biophysique et médecine nucléaire
M.	**AIDE Nicolas**	Biophysique et médecine nucléaire
M.	**ALLOUCHE Stéphane**	Biochimie et biologie moléculaire
M.	**ALVES Arnaud**	Chirurgie digestive
M.	**AOUBA Achille**	Médecine interne
M.	**BABIN Emmanuel**	Oto-Rhino-Laryngologie
M.	**BÉNATEAU Hervé**	Chirurgie maxillo-faciale et stomatologie
M.	**BENOIST Guillaume**	Gynécologie - Obstétrique
M.	**BERGER Ludovic**	Chirurgie vasculaire
M.	**BERGOT Emmanuel**	Pneumologie
M.	**BIBEAU Frédéric**	Anatomie et cytologie pathologique
Mme	**BRAZO Perrine**	Psychiatrie d'adultes
M.	**BROUARD Jacques**	Pédiatrie
M.	**BUSTANY Pierre**	Pharmacologie
Mme	**CHAPON Françoise**	Histologie, Embryologie
Mme	**CLIN-GODARD Bénédicte**	Médecine et santé au travail
M.	**DAMAJ Ghandi Laurent**	Hématologie
M.	**DAO Manh Thông**	Hépatologie-Gastro-Entérologie
M.	**DEFER Gilles**	Neurologie
M.	**DELAMILLIEURE Pascal**	Psychiatrie d'adultes
M.	**DENISE Pierre**	Physiologie
Mme	**DOLLFUS Sonia**	Psychiatrie d'adultes
M.	**DREYFUS Michel**	Gynécologie - Obstétrique
M.	**DU CHEYRON Damien**	Réanimation médicale
Mme	**ÉMERY Evelyne**	Neurochirurgie
M.	**ESMAIL-BEYGUI Farzin**	Cardiologie
Mme	**FAUVET Raffaèle**	Gynécologie – Obstétrique
M.	**FISCHER Marc-Olivier**	Anesthésiologie et réanimation

M. GÉRARD Jean-Louis	Anesthésiologie et réanimation
M. GUILLOIS Bernard	Pédiatrie
Mme GUITTET-BAUD Lydia	Epidémiologie, économie de la santé et prévention
M. HABRAND Jean-Louis	Cancérologie option Radiothérapie
M. HAMON Martial	Cardiologie
Mme HAMON Michèle	Radiologie et imagerie médicale
M. HANOUZ Jean-Luc	Anesthésie et réa. médecine péri-opératoire
M. HULET Christophe	Chirurgie orthopédique et traumatologique
M. ICARD Philippe	Chirurgie thoracique et cardio-vasculaire
M. JOIN-LAMBERT Olivier	Bactériologie - Virologie
Mme JOLY-LOBBEDEZ Florence	Cancérologie
M. JOUBERT Michael	Endocrinologie
M. LAUNOY Guy	Epidémiologie, économie de la santé et prévention
M. LE HELLO Simon	Bactériologie-Virologie
Mme LE MAUFF Brigitte	Immunologie
M. LOBBEDEZ Thierry	Néphrologie
M. LUBRANO Jean	Chirurgie viscérale et digestive
M. MAHE Marc-André	Cancérologie
M. MANRIQUE Alain	Biophysique et médecine nucléaire
M. MARCÉLLI Christian	Rhumatologie
M. MARTINAUD Olivier	Neurologie
M. MAUREL Jean	Chirurgie générale
M. MILLIEZ Paul	Cardiologie
M. MOREAU Sylvain	Anatomie/Oto-Rhino-Laryngologie
M. MOUTEL Grégoire	Médecine légale et droit de la santé
M. NORMAND Hervé	Physiologie
M. PARIENTI Jean-Jacques	Biostatistiques, info. médicale et tech. de communication
M. PELAGE Jean-Pierre	Radiologie et imagerie médicale
Mme PIQUET Marie-Astrid	Nutrition
M. QUINTYN Jean-Claude	Ophtalmologie
Mme RAT Anne-Christine	Rhumatologie
M. RAVASSE Philippe	Chirurgie infantile
M. REPESSE Yohann	Hématologie
M. REZNIK Yves	Endocrinologie
M. ROD Julien	Chirurgie infantile
M. ROUPIE Eric	Médecine d'urgence
Mme THARIAT Juliette	Radiothérapie
M. TILLOU Xavier	Urologie
M. TOUZÉ Emmanuel	Neurologie
M. TROUSSARD Xavier	Hématologie

Mme VABRET Astrid	Bactériologie - Virologie
M. VERDON Renaud	Maladies infectieuses
Mme VERNEUIL Laurence	Dermatologie
M. VIVIEN Denis	Biologie cellulaire

PROFESSEURS ASSOCIÉS DES UNIVERSITÉS A MI-TEMPS

M. DE LA SAYETTE Vincent	Neurologie
Mme DOMPMARTIN-BLANCHÈRE Anne	Dermatologie
M. GUILLAUME Cyril	Médecine palliative
M. LE BAS François	Médecine Générale
M. SABATIER Rémi	Cardiologie

PRCE

Mme LELEU Solveig	Anglais

PROFESSEURS EMERITES

M. HURAULT de LIGNY Bruno	Néphrologie
Mme KOTTLER Marie-Laure	Biochimie et biologie moléculaire
M. LE COUTOUR Xavier	Epidémiologie, économie de la santé et prévention
M. LEPORRIER Michel	Hématologie
M. VIADER Fausto	Neurologie

UNIVERSITÉ DE CAEN · NORMANDIE

UFR SANTÉ - FACULTE DE MEDECINE

Année Universitaire 2019/2020

Doyen
Professeur Emmanuel TOUZÉ

Assesseurs
Professeur Paul MILLIEZ (pédagogie)
Professeur Guy LAUNOY (recherche)
Professeur Sonia DOLLFUS & Professeur Evelyne EMERY (3ème cycle)

Directrice administrative
Madame Sarah CHEMTOB

MAITRES DE CONFERENCES DES UNIVERSITÉS - PRATICIENS HOSPITALIERS

M. ALEXANDRE Joachim	Pharmacologie clinique
Mme BENHAÏM Annie	Biologie cellulaire
M. BESNARD Stéphane	Physiologie
Mme BONHOMME Julie	Parasitologie et mycologie
M. BOUVIER Nicolas	Néphrologie
M. COULBAULT Laurent	Biochimie et Biologie moléculaire
M. CREVEUIL Christian	Biostatistiques, info. médicale et tech. de communication
M. DE BOYSSON Hubert	Médecine interne
Mme DINA Julia	Bactériologie - Virologie
Mme DUPONT Claire	Pédiatrie
M. ÉTARD Olivier	Physiologie
M. GABEREL Thomas	Neurochirurgie
M. GRUCHY Nicolas	Génétique
M. GUÉNOLÉ Fabian	Pédopsychiatrie
M. HITIER Martin	Anatomie - ORL Chirurgie Cervico-faciale
M. ISNARD Christophe	Bactériologie Virologie
M. JUSTET Aurélien	Pneumologie
Mme KRIEGER Sophie	Pharmacie
M. LEGALLOIS Damien	Cardiologie
Mme LELONG-BOULOUARD Véronique	Pharmacologie fondamentale
Mme LEVALLET Guénaëlle	Cytologie et Histologie
M. MITTRE Hervé	Biologie cellulaire
M. SESBOÜÉ Bruno	Physiologie
M. TOUTIRAIS Olivier	Immunologie
M. VEYSSIERE Alexis	Chirurgie maxillo-faciale et stomatologie

MAITRES DE CONFERENCES ASSOCIÉS DES UNIVERSITÉS A MI-TEMPS

Mme ABBATE-LERAY Pascale	Médecine générale
M. COUETTE Pierre-André	Médecine générale
Mme NOEL DE JAEGHER Sophie	Médecine générale
M. PITHON Anni	Médecine générale
M. SAINMONT Nicolas	Médecine générale
Mme SCHONBRODT Laure	Médecine générale

MAITRES DE CONFERENCES EMERITES

Mme DEBRUYNE Danièle	Pharmacologie fondamentale
Mme DERLON-BOREL Annie	Hématologie
Mme LEPORRIER Nathalie	Génétique

Remerciements

Je tiens à remercier très sincèrement,

Monsieur le Pr Denis Agostini, pour m'avoir fait l'honneur d'accepter la présidence de cette thèse. Je le remercie également pour son enseignement tout au long de mon internat. Veuillez recevoir l'expression de ma sincère reconnaissance.

Messieurs les Professeurs Ludovic Berger et Farzin Esmail-Beygui ainsi que Monsieur le Docteur Damien Legallois, pour m'avoir fait l'honneur d'accepter de faire partie du jury et pour l'intérêt que vous avez porté à ce sujet de thèse.

Mon directeur de thèse, le Pr Alain Manrique sans qui ce travail n'aurait jamais été possible. C'est un plaisir de travailler ensemble. Je suis reconnaissant pour ses conseils avisés, son expérience et sa confiance envers moi pour accomplir ce travail.

Toute l'équipe de l'EA4650 du centre Cycéron dans laquelle j'ai pu évoluer dans le cadre de ce travail. Je remercie en particulier Céline Brocquehaye pour son accueil chaleureux et Guillaume Rucher pour notre collaboration. Je remercie Quentin Dupas pour son aide et son humour. Je remercie également chaleureusement le Docteur Christophe Simard pour son soutien, sa disponibilité & son écoute.

L'équipe du CMABio3, Maëlle Guyot et Nicolas Elie pour leurs expertises en Histologie.

Adèle Riot pour ton aide précieuse sur la lecture des lames d'histologie qui a aidé à la mise au point de la technique.

Le Professeur Philippe Delaval, pneumologue et ancien Doyen de la faculté de Médecine de Rennes, qui a incarné pour moi une figure dans mes études supérieures. Je garderai le souvenir de sa sagesse aussi grande que son humilité.

Au Docteur Tanguy Rohou, radiologue, qui m'a fait découvrir et aimer l'Imagerie Médicale par son travail rigoureux et son partage spontané de ses connaissances.

Mes parents pour leurs soutiens et leurs encouragements depuis toujours et durant ces longues années d'études.

Mon frère Gwénolé et ma sœur Aurélie. Merci à tous les deux pour vos conseils, votre écoute et votre soutien. Je suis fier de vos brillants parcours à tous les deux et de ce que vous êtes aujourd'hui.

Tous mes amis, notamment ceux de mon lycée René Cassin, de la faculté de Médecine de Rennes 1 et mes co-internes du C.H.U de Caen qui ont été présents de près comme de loin et qui m'ont permis d'appréhender ce long parcours de manière plus sereine.

Adèle, pour tout ce que tu es. Merci pour ta patience, ton soutien et ton aide si précieuse depuis toutes ces années. A mon tour de t'accompagner pour la fin de ton parcours en Médecine et bien au-delà.

Abréviations

ALP: Alkaline phosphatase

α-MSH: Alpha melana stimulating hormone

ApoE: Apolipoprotein E

AS: Aortic stenosis

ATP: Adenosine tri-phosphate

BMP-2: Bone Morphogenetic Protein 2

CT: Computed tomography

ECG: Electrocardiogramm

ENPP1: Type 1 ectonucleotide phosphodiesterase enzyme

LDL: Low density lipoprotein

Ldlr: Low density lipoprotein receptor

LV: Left ventricle

LVM: Left ventricle mass

MC1R: Melanocortin 1 receptor

MPIO: Micron-sized particles of iron oxide

MR: Magnetic Resonance

NO TT: Group without treatment

NO TT/RT+: Group without treatment but radiation exposure

NO TT/RT-: Group without treatment and without radiation exposure

PBS: Phosphate Buffer Saline

PMMA: Polymethyl methacrylate

PPi: Pyrophosphate inorganic

RA: Rétrécissement aortique

RUNX2: RUNt-related transcription factor 2

SEM: Standard error of the mean

TAVI: Transcatheter aortic valve implantation

TT: Group with treatment

TT/RT+: Group with treatment and with radiation exposure

TT/RT-: Group with treatement and without radiation exposure

VCAM: Vascular Cell Adhesion Molecule

VIC: Valve interstitial cells

WT: Wild Type

Tableaux et figures

Table 1. Left ventricle, left atrium and aorta dimensions assessed using echocardiography at baseline and 3-month follow-up. Measurements were performed in 22 WT and 25 ApoE$^{-/-}$ mice. IVS.: interventricular septum, LVD: left ventricle diameter, LVPW: left ventricle posterior wall, EF: ejection fraction, FS: fractional shortening, LA: left atrium diameter, d: diastole, s: systole. Data are expressed as mean ± SEM.

	Baseline		3 months		p-value			
	WT	ApoE$^{-/-}$	WT	ApoE$^{-/-}$	Global	Time	Genotype	Radiation
IVS.d (mm)	0.72±0.02	0.75±0.01	0.67±0.02	0.68±0.01	0.0009	0.0002	ns	ns
IVS.s (mm)	0.89±0.05	0.8±0.02	0.72±0.02	0.76±0.03	0.01	0.0005	ns	ns
LVDd (mm)	3.70±0.06	3.75±0.09	3.95±0.06	4.12±0.09	<0.01	0.0002	ns	ns
LVDs (mm)	2.48±0.07	2.59±0.08	2.84±0.06	3.13±0.1	<0.0001	<0.0001	0.01	ns
LVPWd (mm)	0.75±0.02	0.86±0.04	0.82±0.03	0.83±0.03	ns	-	-	-
LVPWs (mm)	0.98±0.03	1.07±0.04	0.98±0.03	0.98±0.04	ns	-	-	-
FS (%)	33.13±1.32	31.15±1.08	28.27±0.67	24.40±1.23	<0.0001	<0.0001	<0.01	ns
EF (%)	68.42±1.7	65.30±1.55	61.30±1.08	54.41±2.00	<0.0001	<0.0001	<0.01	ns
LA (mm)	2.17±0.05	2.36±0.07	2.80±0.08	3.15±0.07	<0.0001	<0.0001	0.0003	ns
Aorta (mm)	1.79±0.02	1.86±0.03	1.88±0.04	1.81±0.03	<0.01	ns	ns	0.0001

Table 2. Systolic, diastolic and aortic wall compliance measurements assessed using echocardiography. WT control (n=10), WT 10 Gy (n=6), WT 20 Gy (n=6), ApoE$^{-/-}$ control (n=11), ApoE$^{-/-}$ 10 Gy (n=4) and ApoE$^{-/-}$ 20 Gy (n=10) at 3 months follow-up. Aortic wall compliance was evaluated as the ratio of systolic/diastolic diameter. Data are expressed as mean±SEM, *p<0.05 vs. ApoE$^{-/-}$ 0 Gy.

	WT			ApoE$^{-/-}$			p-value		
Dose	0 Gy	10 Gy	20 Gy	0 Gy	10 Gy	20 Gy	Global	Genotype	Radiation
Systolic diameter (mm)	1.96±0.04	1.82±0.06	1.80±0.09	1.96±0.05	1.83±0.08	1.76±0.05*	0.0129	ns	0.0014
Diastolic diameter (mm)	1.75±0.05	1.67±0.07	1.65±0.09	1.78±0.04	1.73±0.1	1.65±0.05	ns	ns	-
Compliance	1.12±0.01	1.09±0.02	1.08±0.02	1.10±0.02	1.06±0.02	1.07±0.02	0.035	ns	0.0267

Table 3 Effects of PPi administration on left ventricle and aortic dimensions assessed using echocardiography at baseline, 3 months and 5 months of follow-up. N: mice number, IVS: interventricular septum, LVD: left ventricle diameter, LVPW: left ventricle posterior wall, EF: ejection fraction, FS: fractional shortening, LA: left atrium diameter, d: diastole, s: systole. Data are expressed in mean ± SEM.

	Baseline		3 months		5 months		p-value			
	NO TT n=16	TT n=16	NO TT n=16	TT n=15	NO TT n=7	TT n=8	Global	Time	PPi	Radiation
IVSd (mm)	0.81±0.028	0.86±0.037	0.89±0.029	0.84±0.042	0.97±0.064	0.91±0.031	0.0237	0.0844	0.0470	ns
IVSs (mm)	0.97±0.036	1.20±0.035	1.2±0.034	1.3±0.058	1.3±0.11	1.4±0.076	< 0.001	< 0.001	0.0006	ns
LVDd (mm)	3.31±0.09	3.37±0.062	3.6±0.062	3.5±0.13	3.9±0.074	3.9±0.095	ns	0.0012	ns	ns
LVDs (mm)	1.91±0.12	2.05±0.057	2.4±0.061	2.2±0.14	2.7±0.14	2.6±0.14	< 0.068	0.0007	ns	ns
LVPWd (mm)	0.88±0.035	0.99±0.059	0.97±0.061	1.1±0.10	0.89±0.036	0.90±0.033	ns	ns	0.0037	ns
LVPWs (mm)	1.23±0.056	1.29±0.059	1.3±0.053	1.3±0.11	1.2±0.043	1.2±0.057	ns	ns	0.0467	ns
FS (%)	42.99±2.44	39.03±1.51	35±1.1	37±1.9	31±3.0	34±2.3	0.0677	0.0025	ns	ns
EF (%)	79.69±2.2	75.49±1.9	71±1.4	73±2.3	65±4.3	70±2.9	ns	0.0027	ns	ns
Aorta (mm)	1.708±0.035	1.652±0.034	1.823±0.041	1.739±0.043	1.824±0.082	1.755±0.037	0.0317	0.006	0.005	ns

Table 4. Effect of preventive PPi on the aortic root assessed using echocardiography. Aortic wall compliance was calculated as the ratio of systolic/diastolic diameter.

	NO TT		TT		p-value			
	RT- (n=8)	RT± (n=8)	RT- (n=7)	RT± (n=8)	Global	Time	PPi	Radiation
Systolic diameter (mm)	1.8±0.037	1.9±0.075	1.8±0.078	1.7±0.047	0.0317	0.006	0.005	ns
Diastolic diameter (mm)	1.5±0.037	1.6±0.081	1.5±0.051	1.5±0.047	0.0048	0.0004	ns	ns
Compliance	1.2±0.015	1.1±0.033	1.2±0.055	1.2±0.033	ns	ns	0.045	ns

Table 5. Functional aortic valve assessment using echocardiography. Data are expressed as mean±SEM, *p<0.05 vs. ApoE-/- and §p<0.05 vs. dose-equivalent WT.

	WT			ApoE$^{-/-}$			p-value		
Dose	0 Gy	10 Gy	20 Gy	0 Gy	10 Gy	20 Gy	Global	Genotype	Radiation
Flow velocity (cm/s)	184±5	213±10	214±2	261±17§	308±20§	312±15*§	<0.0001	<0.0001	<0.001
Mean gradient (mmHg)	6.33±0.46	8.53±0.93	8.83±0.44	13.58±1.69§	16.92±1.71§	20.57±2.04§*	<0.0001	<0.0001	<0.01
Max gradient (mmHg)	13.68±0.78	18.36±1.88	18.45±0.4	28.05±3.53§	38.57±5.02§	39.75±3.84§	<0.0001	<0.0001	<0.01

Table 6. Functional aortic valve assessment at 3 months according to preventive PPi treatment. Data are expressed in mean±SEM, *p<0.05 vs. NO TT/RT- , §p<0.05 vs. NO TT/RT+, †p<0.05 vs. baseline equivalent subgroup, N: Mice number.

	NO TT		TT		p-value		
	RT- (n=8)	RT± (n=8)	RT- (n=7)	RT± (n=8)	Global	PPi	Radiation
Flow velocity (cm/s)	253±36	354±36†	180±8.5*	184±9.4§	< 0.0001	< 0.0001	0.0492
Mean gradient (mmHg)	18±5.2	31±6.5	6.7±0.92	7.5±1.1	0.0021	0.0002	0.0617
Max gradient (mmHg)	29±8.4	54±11†	13±1.3*	14±1.4§	0.0008	< 0.0001	0.0283

Table 7. Preventive effect of PPi administration on MRI results. Data are expressed as mean±SEM and are indexed to the weight of the animal. LVM: left ventricle mass, EDV: end diastolic volume, ESV: end systolic volume, SV: stroke volume, EF: ejection fraction.

	NO TT		TT		p-value			
	RT- (n=8)	RT± (n=8)	RT- (n=7)	RT± (n=8)	Global	Time	PPi	Radiation
LVM (mg/g)	3.434±0.14	3.7±0.12	2.6±0.91	2.8±0.13	<0.0001	0.0141	0.0013	ns
EDV (µl /g)	2.437±0.16	2.451±0.15	2.8±0.079	2.80±0.2	0.0054	0.0041	0.0658	ns
ESV (µl /g)	1.08±0.1	1.225±0.125	1.5±0.093	1.7±0.19	0.0006	0.0002	0.047	ns
SV (µl /g)	0.0013±0.0001	0.0013±0.0001	0.0013±0.0001	0.0013±7.5^{e}-005	ns	ns	ns	ns
EF (%)	55.78±2.18	55.78±2.18	47±3.4	48±3.7	0.0002	<0.0001	0.0838	0.0328

Table 8. Proportion of MPIO - αVCAM-1 binding using MR imaging in aortic valve leaflets and aortic sinus. MPIO-αVCAM-1 results in T2* signal void on aortic valve leaflets and aortic sinus.

WT				ApoE			
Valve leaflets							
MPIO-VCAM	-	+	Total	MPIO-VCAM	-	+	Total
RT-	2	0	2	RT-	2	0	2
RT+	0	7	7	RT+	3	4	7
Total	2	7	9	Total	5	4	9
Aortic sinus							
MPIO-VCAM	-	+	Total	MPIO-VCAM	-	+	Total
RT-	2	0	2	RT-	2	2	4
RT+	3	4	7	RT+	1	9	10
Total	5	4	9	Total	3	11	14

Table 9. Histologic assessment. Fibrosis was assessed using Picro-Sirius red staining and mineralization process using von Kossa staining. Fibrosis corresponds to the ratio between Picro-Sirius red area and left ventricular area and von Kossa area to the % of von Kossa staining in the aortic valve leaflets area. All the parameters were assessed in 4 WT RT-, 3 WT 10 Gy, 3 WT 20 Gy, 4 $ApoE^{-/-}$ RT-, 4 $ApoE^{-/-}$ 10 Gy and 3 $ApoE^{-/-}$ 20 Gy. Data are expressed as mean ± SEM, *p<0.05 vs. ApoE RT- †p<0.05 vs. ApoE 10 Gy §vs. dose-equivalent WT.

	RT-	10	20	RT-	10	20	Global	Genotype	Radiation
Fibrosis (%)	10.25±0.01	8.83±0.02	11.72±0.01	5.89±0.01	14.30±0.02	9.68±0.02	<0.05	ns	<0.05
Leaflet area (mm^2)	0.144±0.006	0.161±0.015	0.166±0.015	0.115±0.005	0.164±0.008*	0.195±0.019*	0.0001	ns	0.0001
Sinus tissue area (mm^2)	0.253±0.010	0.245±0.009	0.217±0.022	0.473±0.030§	0.484±0.026§	0.697±0.034*†§	<0.0001	<0.0001	<0.05
Von Kossa Area (%)	4.187 ±11.7	3.809±4.4	5.224±1.62	4.224±6.76	7.027±10.287*	4.027±4.584*†	<0.0001	ns	<0.0001

Table 10. Correlation between aortic valve function using echocardiography and histological analysis. p and r values of logistic regression analysis between transaortic flow velocity, mean gradient and aortic wall compliance with von Kossa area (mineralization), leaflet area and aortic sinus lesion.

	Flow velocity		Mean gradient		Aortic wall compliance	
	r	p	r	p	r	p
Mineralization	0.57	<0.01	0.55	0.02	0.47	<0.05
Leaflet area	0.65	0.002	0.62	<0.001	0.48	<0.05
Aortic sinus lesion	0.55	0.02	0.60	<0.01	ns	ns

Table 11. Histologic assessment. Fibrosis was assessed using Picro-Sirius red staining and mineralization process using von Kossa staining. Fibrosis correspond to the % of red staining in the leaflet tissue area. Von Kossa area correspond to the % of von Kossa in the aortic leaflet area. Alizarin red area correspond to the % of red staining in the aortic leaflet area Data are expressed in mean ± SEM.

	NO TT		TT		p-value		
	RT-	RT+	RT-	RT+	Global	PPi	Radiation
Fibrosis (%)	13.55±0.968	12.19±0.956	13.75±1.532	12.88±0.673	ns	ns	ns
Leaflet area (mm^2)	0.157±0.02	0.157±0.02	0.130±0.013	0.174±0.021	ns	ns	ns
Sinus tissue area (mm^2)	1.096±0.142	1.132±0.114	1.048±0.1	0.969±0.111	ns	ns	ns
Von Kossa Area (%)	0.977±0.1808	2.384±0.2465	1.930±0.3413	1.135±0.2166	0.0003	ns	ns
Alizarin Red Area (%)	0.0721±0.025	0.0979±0.045	0.0459±0.016	0.2112±0.117	ns	ns	ns

Figure 1. Planning of radiation exposure. Irradiation consisted of 2 X-ray beams of 2 mm diameter with an angle of 45° and 135°.

(A) Axial view. (B) Sagittal view. (C) Frontal view. (D) Relative dose calculation.

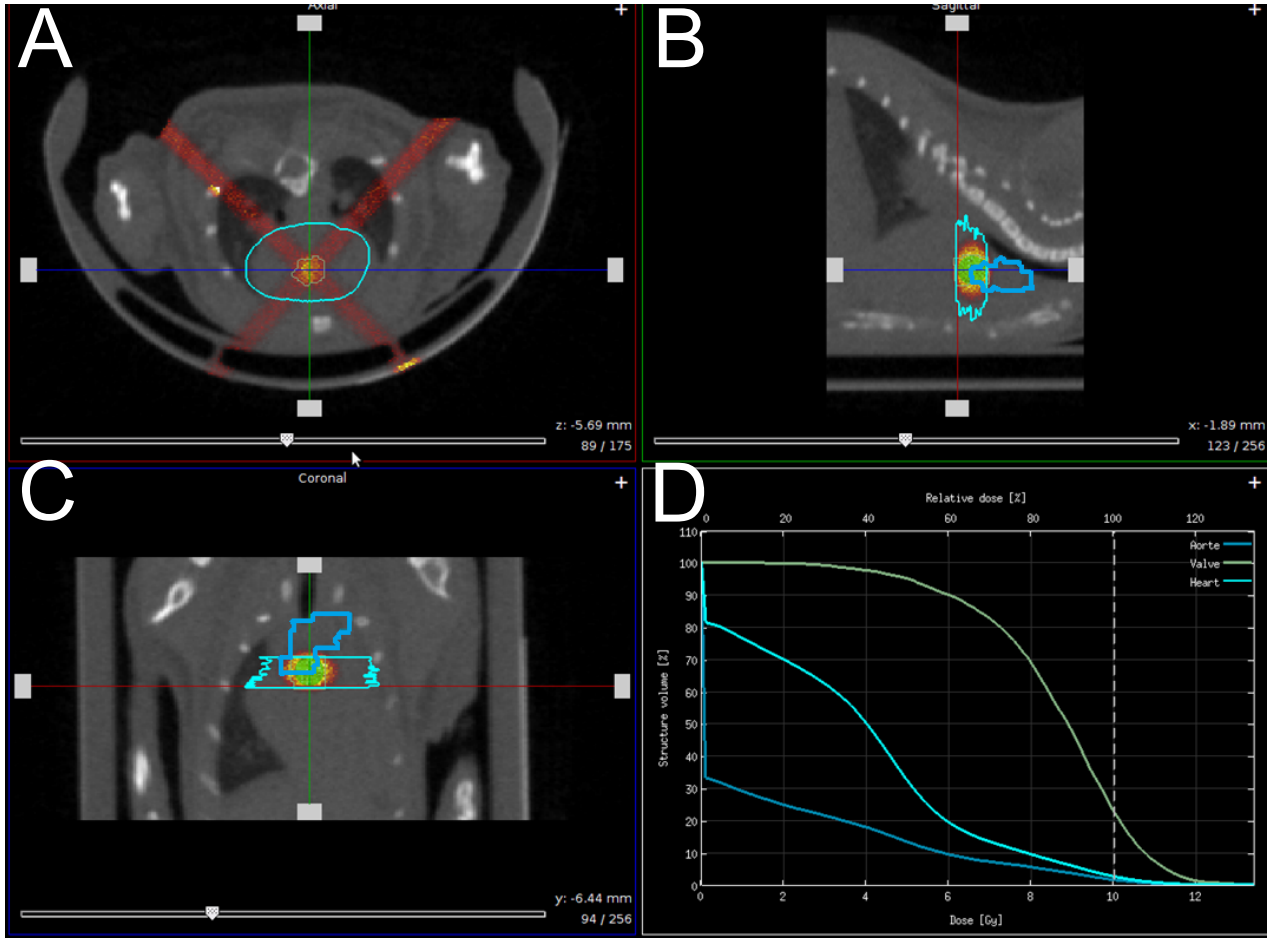

Figure 2. Impact of radiation exposure dose on aortic valve functional assessment using echocardiography. The analysis was performed in WT control (n=10), WT 10 Gy (n=6), WT 20 Gy (n=6), ApoE$^{-/-}$ control (n=11), ApoE$^{-/-}$ 10 Gy (n=4) and ApoE$^{-/-}$ 20 Gy (n=10). A. Transaortic flow velocity. B. Transaortic mean gradient. C. Transaortic maximal gradient. Data are expressed in mean±SEM, *p<0.05 vs. ApoE RT-, §vs. dose-equivalent WT.

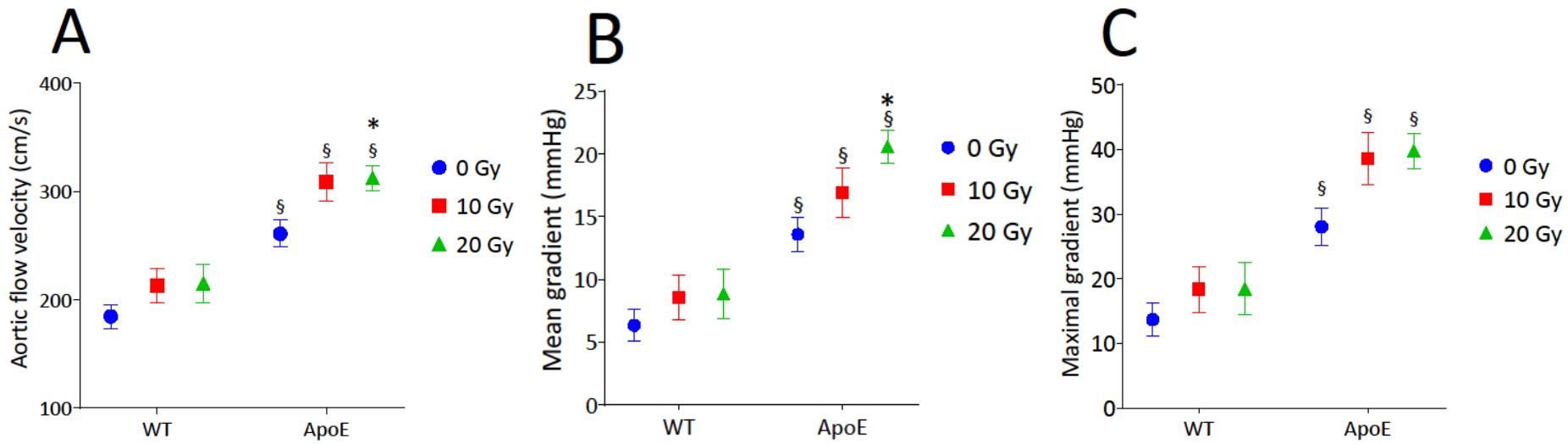

Figure 3. Correlation between von Kossa area and transaortic flow velocity, mean gradient and aortic wall compliance.

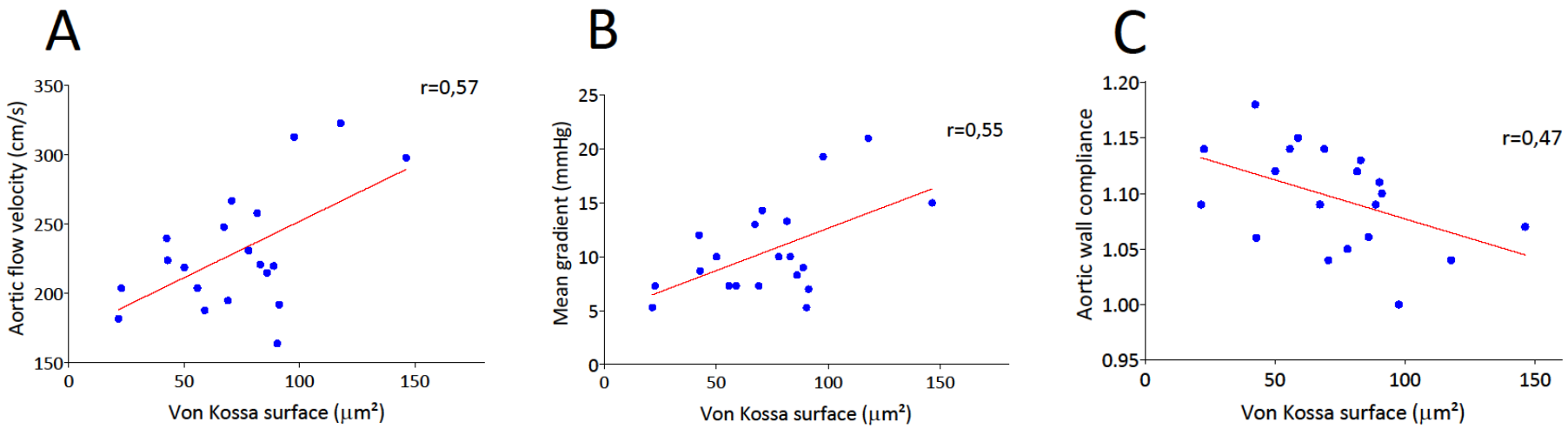

Figure 4. Impacts of radiation and PPi on evolution of velocity flow using echocardiography. Analysis found a global effect (p< 0.0001), radiation (p= 0.0492) and PPi effect (p< 0.0001). (A) Radiation was responsible of an increase of maximum flow velocity in NO TT/ RT+ mice whereas no increase was found with PPi in TT / RT+ mice. (B) No significant variation was found without radiation. ** p< 0.002; *** p< 0.001.

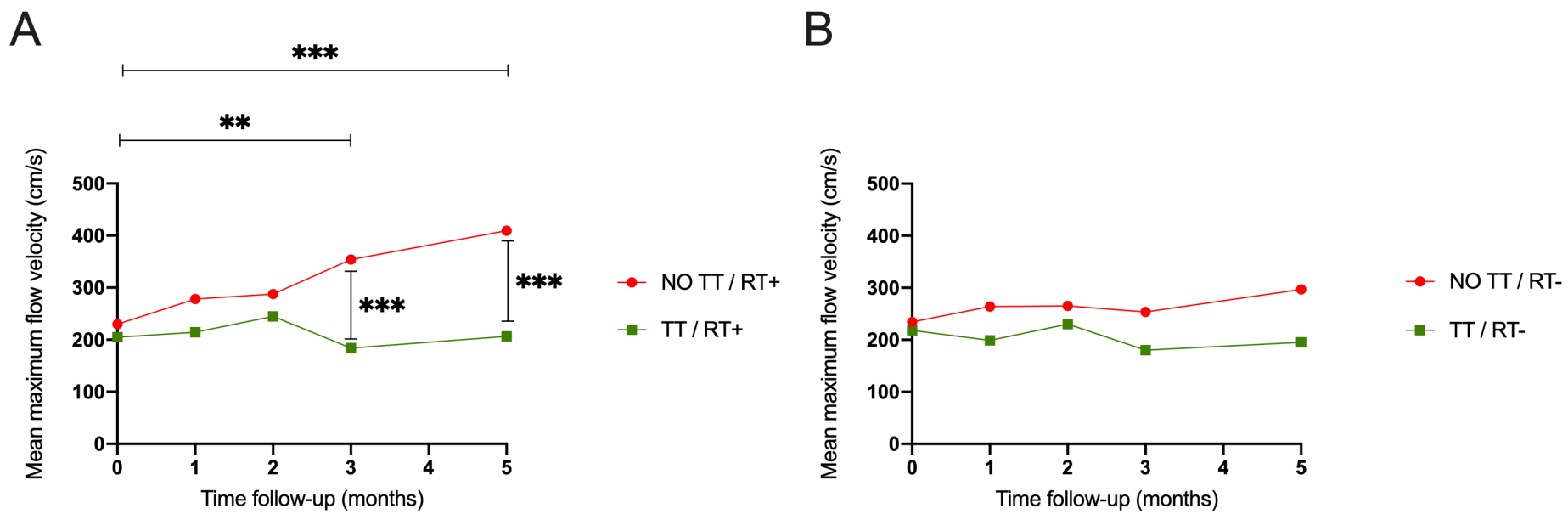

Figure 5. Impacts of radiation and PPi on aortic leaflets using von Kossa staining histological assessment. Analysis found a global effect (p= 0.0003) with interaction between radiation and PPi (p<0.0001). Radiation was responsible of an increase of von Kossa staining in mice without PPi (p= 0.0007). No effect of radiation was found with mice treated by PPi. Comparing mice with radiation, PPi was responsible of a decrease of von Kossa staining (p= 0.0057). * p< 0.05; ** p< 0.002.

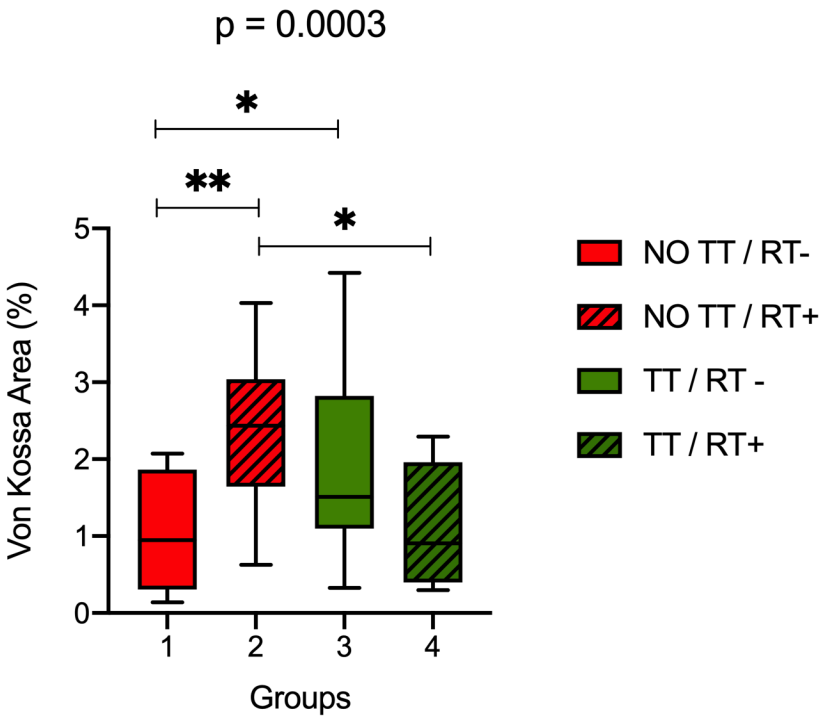

Sommaire

Introduction 1

Material and methods 3

Animals 3

Three-dimensional anatomic atlas of aortic valve 3

Irradiation protocol 4

Echocardiography 5

Cardiac MR imaging 5

Histological analysis 6

Statistical analysis 7

Results 8

Echocardiography 8

Valve function assessment 9

MR morpholgic imaging findings 10

α-VCAM MPIO MR imaging findings 10

Histological analysis 10

Discussion 12

Conclusion 16

Funding 17

Préambule

Le rétrécissement aortique (RA) est la valvulopathie la plus fréquente. Son évolution est inéluctable avec un pronostic sombre en absence de traitement. Le remplacement prothétique valvulaire est l'unique option efficace. Pour les patients non candidats à ce type de prise en charge, l'absence de traitement médical efficient en font actuellement un problème de santé publique majeur. Le développement de nouveaux agents est primordial et passe par l'évaluation préclinique chez l'animal. Or, l'évaluation de nouvelles stratégies thérapeutiques souffre d'un manque de modèles précliniques fiables et reproductibles du RA. Il apparaît donc nécessaire de développer un nouveau modèle pour évaluer de nouveaux agents thérapeutiques.

Mon projet dans le cadre de ma thèse d'exercice en Médecine s'est inscrit dans la suite du développement d'un modèle préclinique de RA au sein de l'EA4650 par Mr Guillaume Rucher & le Pr Alain Manrique. Ce modèle s'est basé sur des études ayant démontré une association entre le RA et la radiothérapie. Pour induire le RA, une irradiation ciblée de la valve aortique a été effectuée chez des souris transgéniques $ApoE^{-/-}$ présentant une athérosclérose accélérée. Les résultats obtenus étaient en faveur d'un RA.

Mon objectif principal était d'évaluer l'efficacité d'une thérapeutique préventive chez ce modèle. À ce titre, j'ai rédigé la saisine du projet #18217 dans une étude comportant 60 souris $ApoE^{-/-}$ réparties en groupe contrôle vs. traité. J'ai eu recours à l'irradiation ciblée de la valve aortique chez la souris $ApoE^{-/-}$ (10Gy) afin de sensibiliser les mécanismes de minéralisation. Afin de tenter de ralentir l'évolution du RA, le pyrophosphate inorganique (PPi) a été choisi comme agent thérapeutique potentiel. Ce choix s'est basé sur la littérature, montrant le développement de calcifications ectopiques au sein des tissus mous et notamment vasculaires dans des pathologies caractérisées par un déficit en PPi. Cela suggérait un rôle majeur du PPi sur la minéralisation. Ce rôle s'est confirmé par des études in vitro et in vivo sur des lésions aortiques et myocardiques. Le second objectif était également de démontrer la reproductibilité du modèle radique de RA pour venir conforter les résultats préliminaires.

Introduction

Aortic stenosis (AS) is the most common form of valvular heart disease in developed countries(1), affecting between 25% of patients over 65 years old and 40% over 80 years old (2,3). Given the lack of prevention strategies aimed at reducing the disease progression, surgical valve replacement was the unique therapeutic alternative until the recent development of revolutionary approach based on percutaneous transcatheter aortic valve implantation (TAVI) (4). However, not all the patients are candidates percutaneous intervention and despite numerous trials, no medical therapy demonstrated its ability to slow down the disease progression marked by high mortality in this case (5).

The early pathophysiological mechanisms involve mechanical lesions, chronic inflammation, and osteogenic phenotypic changes of valve interstitial cells inducing progressive mineralization (6) that is central to the development of this disease. The development of new preventive or therapeutic strategies suffers from the lack of reliable and reproducible preclinical models of calcified aortic stenosis. Documented preclinical models are mainly based on accelerated atherosclerosis in $Ldlr^{-/-}$ and $ApoE^{-/-}$ mice submitted to high fat diet. Clinical studies demonstrated that mediastinal radiation therapy may induce various cardiac damage including calcified AS (7). In addition, recent *in vitro* experiments demonstrated that irradiation of human aortic valve interstitial cells (VIC) induced the expression of osteogenic factors 24h after irradiation such as Bone Morphogenetic Protein 2 (BMP-2), alkaline phosphatase (ALP) and Runx2 that are necessary for bone formation (8).

Inorganic pyrophosphate (PPi) is a metabolite naturally present in the human body and produced by the hepatic type 1 ectonucleotide phosphodiesterase enzyme (ENPP1) from adenosine tri-phosphate (ATP) supplied by the transporter ABCC6 (9). Previous data emphasized the role of PPi in the inhibition of ectopic mineralization resulting from generalized arterial calcification of infancy with deficiency of ENPP1 or from pseudoxanthoma elasticum with ABCC6 mutation (9). Several in vitro and in vivo studies have confirmed this role, including in cardiac and aortic tissues (10,11), and suggested that a direct binding of the PPi to the hydroxyapatite crystals could prevent their aggregation, selectively stopping the process of ectopic mineralization.

Based on these findings, the aim of this study was to assess the feasibility of inducing a calcified AS using targeted aortic valve irradiation in mice, and to evaluate the impact of a therapy using PPi to prevent aortic stenosis in this model.

Material and methods

Animals

The institutional animal ethics committee approved the animal experiments (Cenomexa #12314 and #18217). A total of 21 animals were randomly allocated to 10 Gy or 20 Gy for both genotype (WT 10 Gy, n=6; WT 20 Gy, n=6; ApoE 10 Gy, n=4; and ApoE 20 Gy, n=10). The control animals were distributed in 2 groups of C57Bl6/J (n=10, WT RT-) and ApoE$^{-/-}$ mice (n=11, ApoE RT-). To assess the impact of PPi in preventing AS, 60 animals were randomized to receive PPi (n = 30, TT) or not (n = 30, NO TT), and further randomly allocated to 2 subgroups, consisting of a 10 Gy iraddiation to the aortic root (TT/RT+, NO TT/RT+) and non-irradiated (TT/RT-, NO TT/RT-) subgroups. All animals were maintained *ad libitum* with a standard chow diet composed by 8.4% fat, 19.3% protein, 72.4% carbohydrates, 0.55% phosphorus, 0.73% calcium, 0.16% magnesium, 1000 UI/kg vitamin D3. The TT mices, received PPi ordered in the form of hydrated powder (Sigma Aldrich Chemistry Laboratory; F-38297 St Quentin Fallavier, France) in free distribution via drinking water at a concentration of 10 mM. The PPi solution was renewed every 3 days. The pH was adjusted on standard drinking water by adding hydrochloric acid. PPi administration was started on the day of irradiation until death in the TT/RT+ mices.

Three-dimensional anatomic atlas of aortic valve

To target the aortic valve during irradiation, we built a murine cardiac atlas using MR data. MR experiments were carried out using a 7T magnet (Pharmascan® Bruker, Billerica, USA). T1 Flash MR images were performed in 13 male C57Bl6/J mice 16-week-old) using a strict axial multi-slice sequence encompassing the heart: TR/TE

176.6/4.2 ms, 20 slices, 6 repetitions. Automatic alignment and fusion of the 6 repetitions were performed using ImageJ software (version 1.52a, Bethesda, MD) to obtain one single image series for each animal. Aortic valve and aorta from the insertion to aortic isthmus were segmented. Then, a threshold set to 75% of co-localization of each aortic valve segmentation was performed to determine the aortic valve segmentation on the atlas. The same method was used for the aorta segmentation.

Irradiation protocol

Anesthesia was induced with 5% isoflurane gas (Forene®, AbbVie, Rungis, France) and maintained with isoflurane 2% gas in a mixed of O_2 and N_2O (1:2) and animals were placed in prone position in a dedicated bed. Computed tomography (CT) was performed encompassing the chest (80 kV, 0.5 mA). Using 3D Slicer software (www.slicer.org), cardiac atlas was manually aligned with CT acquisition to localize the aortic valve and the aorta with segmentations using trachea and bronchia bifurcation as anatomical markers. Planning of radiation exposure was performed using SmartPlan® (Precision X-ray Inc., North Brandford, CT). Tissues (air, lung, soft tissue, bone) were segmented using Hounsfield units. Irradiation consisted of 2 beams of 2 mm diameter with an angle of 45° and 135° (Figure 1). The spatial resolution and dose distribution was previously assessed using polymethyl methacrylate (PMMA) phantoms. The animals randomized to receive radiation therapy underwent a targeted irradiation on the aortic valve at a dose of 10 Gy using a Pxi225CX micro-irradiator (Precision X-ray Inc, North Brandford, CT) in a single fraction (2.22 Gy/min, 225 kV, 13 mA, 0.3 mm copper filter).

Echocardiography

Echocardiography was performed at baseline and 3-month follow-up in isoflurane anesthetized mice with a heart rate <450 beats/min using Philips iE33 (Philips Healthcare, Best, Netherlands) and linear ultrasound probe L15-7io (128 elements, 7-15 MHz). Aortic valve function was assessed using pulse wave Doppler-mode that measures transaortic flow velocity and mean gradient. M-mode images of the parasternal long and short axis views were used to measure left ventricle and aortic root dimensions. In addition, 16 animals randomized to PPi treatment or placebo underwent addition echocardiography assessment at 2 months and 5-month follow-up. The mean of 3 measurements for each parameter was calculated.

Cardiac MR imaging

Morphogical evaluation in cardiac MR only concerned the effects of preventive PPi. Eight animals from each subgroup (n = 32) had a follow-up imaging. MRI was performed using a 7T magnet (Pharmascan® Bruker, Billerica, USA) with dual respiratory and ECG gating with a heart rate < 500 beats/min. It was performed at baseline then 1^{st}, 3^{rd} (n = 32) and 5^{th} month (n = 16) from radiation exposure or PPi introduction. A multi-slice black blood intragate flash sequence was used: thickness of the sections of 560 µm, field of view: 28 × 28 mm, size of the matrix: 128 × 128 , spatial resolution: 0.219x0.219 mm / pixel, 20 images / cardiac cycle, TE / TR: 2/73, tilt angle: 25 °. According to the animal and its growth, the number of slices were adapted to the heat size and could varied from 8 to 11. The post image processing was done using the software Segment © version 2.0. A manual segmentation of the two ventricles contours were done at the endocardial and epicardial level in telesystole and telediastole in order to calculate the left ventricular volumes, ejection fraction and

mass. Left ventricular mass and volumes were indexed to the animal body weight measured just before each examination. To evaluate endothelial activation, MR imaging without and with intravenous injection of 200 µL of micron-sized particles of iron oxide (MPIO) (DynaBeads MyOnes Tosyl Activated, ThermoFisher Scientific, Waltham, USA) conjugated with specitic αVCAM-1 antibodies (clone A(429), BD BioScience, Franklin Lakes, USA) were used by incubation at 37°C for 48h. Telediastolic T2* weighted MR images were acquired using a multi-slice sequence: field of view: 1809 x 939 mm2, TR/TE 100/4.25 ms, 12 slices, voxel: 0.1x0.1x0.15 mm3 encompassing the thoracic aorta were performed were performed in 2 WT RT-, 4 WT 10 Gy, in 3 WT 20 Gy, in 4 $ApoE^{-/-}$ RT-, in 4 $ApoE^{-/-}$ 10 Gy and in 6 $ApoE^{-/-}$ 20 Gy mice. MRI images were analysed using Osirix v.6.5.2 software. MPIO-αVCAM-1 binding results in a T2* signal void in the lumen of the vasculature.

Histological analysis

AS mode validationl:

Mice were sacrificed 3 months after their inclusion in the study. Heart were dissected after the injection of 300 µL of KCl 1 M under a microscope, perfused with heparinized (50 U/mL) Phosphate Buffer Saline 5/100 (PBS) and cryomounted in optimal cutting embedding medium (CellPath, ThermoFisher Scientific, Waltham, USA). For each animal, eight 10-µm-thick slices were collected. Cryosections were placed in 5% silver nitrate solution for 30-60 min then fixed in 5% sodium-thiosulfate solution for 2-3 min. Sections were parallel to the valve plane and digitized using ScanScope CS (Leica Byosystems, Wetzlar, Germany). Tissue segmentation was manually performed using Aperio ImageScope software v12.3 (Leica Biosystem, Wetzlar, Germany). Aortic valve leaflet area, von Kossa area, the number of independent von Kossa structures and the tissue aortic sinus area were assessed.

Preventive effects of PPi:

Mice were sacrified 7 months after their inclusion in the study. The heart dissection technique was performed in identical conditions as in the AS model except that the heart was weighed and fixed in formalin. Finally, section of hearts was perpendicular to the valve plane. Sections were digitized and post processed as described in the AS model study. In addition to von Kossa staining to assess mineralization process, Alizarin red staining was used.

Statistical analysis

Values were expressed as mean ± SEM. A linear model analysis was used to evaluate the effect of the post-radiation time, the genotype and the radiation dose. Post-hoc analysis was performed using Tukey HSD test. A logistic regression analysis was used to correlate the quantitative analysis of von Kossa staining and sinus lesion area with mean aortic gradient, aortic valve flow velocity and aortic wall compliance. For proportions, the chi-square test was used to compare differences between groups. Statistical analyses were performed using JMP 11 (SAS Institute, Cary, NC). A p value ≤ 0.05 was considered statistically significant.

Results

Radiation exposure was well tolerated in all animals. The animals' weight remained stable during all the study.

Echocardiography

AS model validation:

Table 1 summarizes echocardiographic findings. There was a left ventricle enlargement associated with an interventricular septum thinning and a decreased systolic function at 3 months follow-up. However, there was no impact of radiation on these functional parameters, except on the aortic root diameter that was lower in animals submitted to radiation exposure. Aortic root compliance at 3-month follow-up was significantly impaired after radiation therapy, related to a decrease in systolic aortic diameter (Table 2).

Preventive effects of PPi:

Table 3, summarizes echocardiographic findings. Over time there was a left ventricle enlargement associated with an interventricular septum systolic thinning, an increase in diastolic and systolic diameters. An increased interventricular septum thickness was found in TT mice at baseline after randomization, and throughout follow-up. Regarding the left ventricular ejection fraction (LVEF), a decrease was observed over time, from the 2th month of follow-up. Although there was no global effect of radiation exposure and PPi, in multivariate analysis, a LVEF decrease over time was only observed in NO TT / RT+ mice at 3-month ($p= 0.044$) and 5-month ($p= 0.0058$) follow-up vs. baseline. No significant difference was observed in TT / RT+ over time.

The systolic function also decreased in the NO TT/RT- subgroup at 5-month vs. baseline (p= 0.0267). Regarding aortic root diameter and compliance, no effect of radiation exposure was observed (Table 4). The global effect from PPi on aortic compliance (p= 0.045) should be interpreted with caution. Indeed results were only significant at baseline and 1st month of follow-up, then no difference were found between TT and NO TT.

Valve function assessment

As model validation:

The aortic flow velocity and the trans-aortic valvular gradients were significantly higher in ApoE$^{-/-}$ mice (p<0.0001, Table 5). However, radiation therapy resulted in a further increase of aortic flow velocity (p<0.001) and valvular gradients (p<0.01), especially in ApoE$^{-/-}$ mice. As shown in Figure 2, the impact of radiation on trans-aortic Doppler findings was dose-dependent.

Preventive effects of PPi:

A global effect of PPi was observed (Table 6), leading to a stability over the time in maximum (p< 0.0001; Figure 4) and mean flow velocity (p< 0.0001). The same results were observed for maximal (p< 0.0001) and mean gradients (p= 0.0002). The global effect of radiation was responsible for an increase in aortic maximum flow velocity (p= 0.0492) and maximal gradient (p= 0.0283) especially in NO TT / RT+ mice. Indeed, in NO TT/RT+, there was a significant increase in maximal flow velocity at 3-month (p= 0.0015) and 5-month follow-up (p= 0.0002) vs. baseline. However, no significant difference was found in TT/RT+ and TT/RT- mice over time. No aortic regurgitation was noted.

MR morphologic imaging findings

Preventive PPi resulted in a decreased left ventricular mass (Table 7), with a significant difference observed at 3-month follow-up between TT/RT+ and NO TT/RT+ ($p= 0.0005$) and between TT/ RT- vs. NO TT/ RT- ($p= 0.0007$). Regarding EF, ESV and EDV, no significant difference were found.

α-VCAM MPIO MR imaging findings

In RT- animals, α-VCAM MPIO MR imaging was normal in WT mice whereas 5/8 (60%) $ApoE^{-/-}$ demonstrated a T2* signal void (Table 8). The incidence of a T2* signal void was increased in RT+ animals. Logistic regression confirmed that radiation exposure was independently associated to a T2* signal void in the valve leaflets ($p< 0.001$), and that both genotype and radiation exposure were associated to a T2* signal void in the aortic sinus ($p< 0.01$ and $p< 0.05$ respectively).

Histological analysis

AS model validation:

Histological findings showed that, independently of radiation exposure, $ApoE^{-/-}$ mice had an increased aortic sinus lesion area compared to WT (Table 9). In addition, there was a significant remodeling of valve leaflets and aortic sinus lesion related to radiation exposure, especially in $ApoE^{-/-}$ mice. This remodeling further increased with the radiation dose in $ApoE^{-/-}$. Von Kossa staining increased after radiation exposure in valve leaflets ($p<0.001$), especially in $ApoE^{-/-}$ mice. Of note, von Kossa staining was decreased in ApoE after 20 Gy compared to 10 Gy. As described in Table 10 and Figure 3, there was a significant correlation between tissue remodeling and both

functional valve parameters and aortic wall compliance. Finally, radiation exposure resulted in left ventricular fibrosis assessed using Picro-Sirius red staining ($p<0.05$).

Preventive effects of PPi:

Histological assessment (table 11) showed a strong interaction between radiation exposure and PPi using von Kossa staining ($p< 0.0001$). Radiation exposure was responsible of an increase of 144% (mean) of von Kossa staining in aortic leaflets area in NO TT mice ($p= 0.0007$) (figure 5). In addition, a decrease of 52% (mean) of von Kossa staining was observed in TT/RT+ vs. NO TT/RT+ mice ($p= 0.0057$). Thus, no significant increase of Von Kossa staining was found in TT mice with radiation exposure. Surprisingly no significant difference was observed for Alizarin and Picro-Sirius red stainings (in leaflet area), leaflet area and sinus tissue area.

Discussion

The main result of this study is that radiation exposure of ApoE$^{-/-}$ mice resulted in an aortic stenosis demonstrated by an increase of aortic flow velocity associated with an increase of von Kossa staining in aortic valve leaflets. In addition, early treatment with PPi prevented the appearance of radiation-induced aortic lesions.

Calcified AS is characterized by fibro-calcific remodeling of valve leaflets. The progression of the disease involves severe calcification within the valve leaflets leading to an impairment of valve motion contributing to a blood flow obstruction (6). The high incidence of valvular dysfunction had been reported in populations undergoing mediastinal radiation therapy (12). The progression of AS is also accelerated in these patients, underlining the potential of X-rays to initiate and develop valvular lesions (13). Previous *in vitro* studies demonstrated that a local 10 Gy irradiation of human aortic valve interstitial cells induced an osteogenic phenotype differentiation (8).To our best knowledge, the present study is the first that evaluated the impact of targeted radiation exposure on the development of a calcified AS in a mouse model.

Calcific deposition has been previously reported in a mouse model of high fat diet-induced AS (14,15). The supplementation of 1.25% of cholesterol, 57.5% kcal fat and 27.4% kcal carbohydrate resulted in valve leaflets thickening with an increase in the sinus lesion volume compared to control mice fed with a normal diet (15). A valve leaflet thickening was also found in Ldlr$^{-/-}$ Apob$^{100/100}$ mice with a 0.15 % cholesterol diet, associated with an increase of aortic valve flow velocity which was rescued by a regular exercise training (16). In our study, although leaflet thickness tended to

increase with the radiation dose, increasing radiation from 10 to 20 Gy in $ApoE^{-/-}$ mice resulted in lower leaflet calcification von Kossa staining. A similar phenomenon was observed with the amount of aortic sinus lesion that further increased with radiation dose, suggesting that active inflammation is responsible for persistent increasing leaflet thickness.

Left ventricular remodeling is a key issue in patients with aortic stenosis (17). Using various preclinical models, previous studies showed an association between aortic valve leaflet remodeling and left ventricular function impairment. A significant decrease of fractional shortening was found in several models (18,19), as well as a left ventricular hypertrophy (18,20–22). In our study, Picro-Sirius red staining showed an increased left ventricular fibrosis after radiation exposure. Moreover, based on MRI findings, it confirmed the presence of LV hypertrophy after radiation exposure. Barrick et al. (18) reported LV hypertrophy and dilation with a decreased FS in $Egfr^{wa2/wa2}$ mice with a higher peak aortic velocity of 370 cm/s. Compared to our results, studies based on high cholesterol diet reported LV hypertrophy in spite of similar aortic velocities (18,20,21).

The second main result from our study concerns the impact of PPi to prevent AS. First, based on echocardiography findings, PPi prevented from increase of trans-valvular aortic velocity while no significant LVEF decrease was found in TT mice in contrary to NO TT mice. Moreover, based on MRI findings, PPi prevented LV hypertrophy. Finally, histological findings showed that PPi prevented the increase of von Kossa staining on aortic leaflets after radiation exposure.

Histological findings highlighted discrepancies in the results concerning the mineralization process using von Kossa staining. First, a lower quantification of von Kossa staining in aortic leaflets from 10 to 20 Gy which may suggests a toxic effect of high dose radiation on the mineralization process, with persistent inflammation as demonstrated by MPIO-αVCAM1 MR imaging. Second a discrepancy between von Kossa and Alizarin red staining should be interpreted with caution. It is documented that melanocytes, from neural crest cells, are consistently found in heart valves, including in aortic leaflets (23), and can be misidentified as calcification using von Kossa staining (24). However, the cardiac function of melanocytes remains poorly understood. The increase of von Kossa staining in NO TT / RT+ was related to radiation exposure. Radiation may induce DNA damage which is responsible for an increase of alpha melanin stimulating hormone (α-MSH), an agonist of the melanocortin 1 receptor (MC1R) (25,26). Activation of MC1R in melanocytes result in melanin secretion. However, the rationale for the absence of increase in TT/RT+ is less clear.

The absence of Alizarin red staining suggest that the observed von Kossa staining variations may be linked to melanin secretion and supports imaging findings as well. Previous findings demonstrated that melanin may affect the mechanical properties of heart valves (27,28). The amount of melanin is strongly and positively correlated with valvular rigidity in mice. In that way, based on our histological findings, increase of von Kossa staining linked to melanin could participate to the increase of transvalvular aortic velocity flow. Melanin is colocalized with a proteoglycan from the spongiosa heart valve matrix, the versican B (27). The rigidity could be due to melanin directly or due to an interaction with the extra cellular matrix as Versican B. Melanocytes produce metalloproteases and could be involved in tissue homeostatis in

interaction with extra cellular matrix as Versican B. This proteglycan play a key role in the neural crest migration as melanoblasts (29,30).

The absence of increase von Kossa staining in TT/RT+ is less clear. We hypothesize that PPi allows to create a protective and less critical environment without the need for melanocyte action. Indeed many role of cardiac melanocytes are known in cardio-vascular field. MC1R is also present in endothelial cells, monocytes and fibroblasts (31,32). These cells play a key role in the regulation of melanogenesis and interact between each other in the skin (33). MC1R is activated by a-MSH which is secreted by melanocytes. The MC1R and a-MSH signaling pathway has a protective role on human aortic endothelial function (34,35), inflammation (32) and atherosclerotic processes (36). It activates a cholesterol efflux transporter in macrophages, reduces oxidized LDL uptake and allows to stabilize atherosclerotic plaques (37). Concerning mineralization process, cell culture showed that a-MSH may also induce osteoblastic differentiation of MC3T3 cells with an increase of ALP expression and RUNX2 activation (38). Based on these arguments, we hypothesize that melanocytes could play a role in the development of aortic valve lesions after X-ray exposure.

Conclusion

This study demonstrated that targeted aortic valve irradiation in ApoE-/- mice resulted in aortic lesions with accelerated transvalvular flow. Early oral administration of PPi prevented the radiation-induced aortic stenosis, and confirm the usefulness of this preclinical model for assessing new therapeutic strategies. Understanding the role of melanocytes in aortic leaflets warrant further investigations.

Funding :

This work was conducted as part of the FHU REMOD-VHF project and supported by the French Government, managed by the National Research Agency (ANR) under the program “Investissements d’avenir” with the reference ANR-16-RHUS-0003.

Bibliographie

1. Nkomo VT, Gardin JM, Skelton TN, Gottdiener JS, Scott CG, Enriquez-Sarano M. Burden of valvular heart diseases: a population-based study. Lancet. 16 sept 2006;368(9540):1005-11.

2. Coffey S, Cox B, Williams MJA. The Prevalence, Incidence, Progression, and Risks of Aortic Valve Sclerosis. Journal of the American College of Cardiology. juill 2014;63(25):2852-61.

3. Stewart BF, Siscovick D, Lind BK, Gardin JM, Gottdiener JS, Smith VE, et al. Clinical Factors Associated With Calcific Aortic Valve Disease. 29(3):5.

4. Cribier A, Eltchaninoff H, Bash A, Borenstein N, Tron C, Bauer F, et al. Percutaneous transcatheter implantation of an aortic valve prosthesis for calcific aortic stenosis: first human case description. Circulation. 10 déc 2002;106(24):3006-8.

5. Marquis-Gravel G, Redfors B, Leon MB, Généreux P. Medical Treatment of Aortic Stenosis. Circulation. 29 nov 2016;134(22):1766-84.

6. Lindman BR, Clavel M-A, Mathieu P, Iung B, Lancellotti P, Otto CM, et al. Calcific aortic stenosis. Nat Rev Dis Primers. 3 mars 2016;2:16006.

7. Raghunathan D, Khilji MI, Hassan SA, Yusuf SW. Radiation-Induced Cardiovascular Disease. Current Atherosclerosis Reports [Internet]. mai 2017 [cité 30 oct 2018];19(5). Disponible sur: http://link.springer.com/10.1007/s11883-017-0658-x

8. Nadlonek NA, Weyant MJ, Yu JA, Cleveland JC, Reece TB, Meng X, et al. Radiation Induces Osteogenesis in Human Aortic Valve Interstitial Cells. J Thorac Cardiovasc Surg. déc 2012;144(6):1466-70.

9. Jansen RS, Duijst S, Mahakena S, Sommer D, Szeri F, Váradi A, et al. ABCC6-mediated ATP secretion by the liver is the main source of the mineralization inhibitor inorganic pyrophosphate in the systemic circulation-brief report. Arterioscler Thromb Vasc Biol. sept 2014;34(9):1985-9.

10. Rathan S, Yoganathan AP, O'Neill CW. The role of inorganic pyrophosphate in aortic valve calcification. J Heart Valve Dis. juill 2014;23(4):387-94.

11. O'Neill WC, Lomashvili KA, Malluche HH, Faugere M-C, Riser BL. Treatment with pyrophosphate inhibits uremic vascular calcification. Kidney Int. mars 2011;79(5):512-7.

12. Wethal T, Lund M-B, Edvardsen T, Fosså SD, Pripp AH, Holte H, et al. Valvular dysfunction and left ventricular changes in Hodgkin's lymphoma survivors. A longitudinal study. Br J Cancer. 18 août 2009;101(4):575-81.

13. Donnellan E, Griffin BP, Johnston DR, Popovic ZB, Alashi A, Kapadia SR, et al. Rate of Progression of Aortic Stenosis and its Impact on Outcomes in Patients With Radiation-Associated Cardiac Disease. JACC: Cardiovascular Imaging. août 2018;11(8):1072-80.

14. Aikawa E, Nahrendorf M, Sosnovik D, Lok VM, Jaffer FA, Aikawa M, et al. Multimodality Molecular Imaging Identifies Proteolytic and Osteogenic Activities in Early Aortic Valve Disease. Circulation. 2007;115(3):377-86.

15. Scatena M, Jackson MF, Speer MY, Leaf EM, Wallingford MC, Giachelli CM. Increased Calcific Aortic Valve Disease in response to a diabetogenic, procalcific diet in the LDLr -/- ApoB 100/100 mouse model. Cardiovascular Pathology. mai 2018;34:28-37.

16. Matsumoto Y, Adams V, Jacob S, Mangner N, Schuler G, Linke A. Regular exercise training prevents aortic valve disease in low-density lipoprotein-receptor-deficient mice. Circulation. 16 févr 2010;121(6):759-67.

17. Lindman BR, Arnold SV, Madrazo JA, Zajarias A, Johnson SN, Pérez JE, et al. The adverse impact of diabetes mellitus on left ventricular remodeling and function in patients with severe aortic stenosis. Circ Heart Fail. mai 2011;4(3):286-92.

18. Barrick CJ, Roberts RB, Rojas M, Rajamannan NM, Suitt CB, O'Brien KD, et al. Reduced EGFR causes abnormal valvular differentiation leading to calcific aortic stenosis and left ventricular hypertrophy in C57BL/6J but not 129S1/SvImJ mice. AJP: Heart and Circulatory Physiology. 2009;297(1):H65-75.

19. Nus M, MacGrogan D, Martínez-Poveda B, Benito Y, Casanova JC, Fernández-Avilés F, et al. Diet-Induced Aortic Valve Disease in Mice Haploinsufficient for the Notch Pathway Effector RBPJK/CSL. Arteriosclerosis, Thrombosis, and Vascular Biology. juill 2011;31(7):1580-8.

20. Drolet M-C, Roussel E, Deshaies Y, Couet J, Arsenault M. A high fat/high carbohydrate diet induces aortic valve disease in C57BL/6J mice. J Am Coll Cardiol. 21 févr 2006;47(4):850-5.

21. Weiss RM, Ohashi M, Miller JD, Young SG, Heistad DD. Calcific aortic valve stenosis in old hypercholesterolemic mice. Circulation. 7 nov 2006;114(19):2065-9.

22. Miller JD, Weiss RM, Serrano KM, Castaneda LE, Brooks RM, Zimmerman K, et al. Evidence for active regulation of pro-osteogenic signaling in advanced aortic valve disease. Arterioscler Thromb Vasc Biol. déc 2010;30(12):2482-6.

23. Levin MD, Lu MM, Petrenko NB, Hawkins BJ, Gupta TH, Lang D, et al. Melanocyte-like cells in the heart and pulmonary veins contribute to atrial arrhythmia triggers. J Clin Invest. 2 nov 2009;119(11):3420-36.

24. Hulin A, Hortells L, Gomez-Stallons MV, O'Donnell A, Chetal K, Adam M, et al. Maturation of heart valve cell populations during postnatal remodeling. Development. 12 2019;146(12).

25. Lin JY, Fisher DE. Melanocyte biology and skin pigmentation. Nature. 22 févr 2007;445(7130):843-50.

26. Suzuki K, Ojima M, Kodama S, Watanabe M. Radiation-induced DNA damage and delayed induced genomic instability. Oncogene. 13 oct 2003;22(45):6988-93.

27. Carneiro F, Kruithof BP, Balani K, Agarwal A, Gaussin V, Kos L. Relationships between melanocytes, mechanical properties and extracellular matrix composition in mouse heart valves. J Long Term Eff Med Implants. 2015;25(1-2):17-26.

28. Balani K, Brito FC, Kos L, Agarwal A. Melanocyte pigmentation stiffens murine cardiac tricuspid valve leaflet. J R Soc Interface. 6 nov 2009;6(40):1097-102.

29. Perissinotto D, Iacopetti P, Bellina I, Doliana R, Colombatti A, Pettway Z, et al. Avian neural crest cell migration is diversely regulated by the two major hyaluronan-binding proteoglycans PG-M/versican and aggrecan. Development. juill 2000;127(13):2823-42.

30. Braunewell KH, Pesheva P, McCarthy JB, Furcht LT, Schmitz B, Schachner M. Functional involvement of sciatic nerve-derived versican- and decorin-like molecules and other chondroitin sulphate proteoglycans in ECM-mediated cell adhesion and neurite outgrowth. Eur J Neurosci. 1 avr 1995;7(4):805-14.

31. Böhm M, Luger TA. The role of melanocortins in skin homeostasis. Horm Res. 2000;54(5-6):287-93.

32. Catania A, Gatti S, Colombo G, Lipton JM. Targeting melanocortin receptors as a novel strategy to control inflammation. Pharmacol Rev. mars 2004;56(1):1-29.

33. Yamaguchi Y, Hearing VJ. Physiological factors that regulate skin pigmentation. Biofactors. avr 2009;35(2):193-9.

34. Rinne P, Nordlund W, Heinonen I, Penttinen A-M, Saraste A, Ruohonen ST, et al. α-Melanocyte-stimulating hormone regulates vascular NO availability and protects against endothelial dysfunction. Cardiovasc Res. 1 févr 2013;97(2):360-8.

35. Saporiti F, Piacentini L, Alfieri V, Bono E, Ferrari F, Chiesa M, et al. Melanocortin-1 Receptor Positively Regulates Human Artery Endothelial Cell Migration. Cell Physiol Biochem. 2019;52(6):1339-60.

36. Rinne P, Silvola JMU, Hellberg S, Ståhle M, Liljenbäck H, Salomäki H, et al. Pharmacological activation of the melanocortin system limits plaque inflammation and ameliorates vascular dysfunction in atherosclerotic mice. Arterioscler Thromb Vasc Biol. juill 2014;34(7):1346-54.

37. Rinne P, Rami M, Nuutinen S, Santovito D, van der Vorst EPC, Guillamat-Prats R, et al. Melanocortin 1 Receptor Signaling Regulates Cholesterol Transport in Macrophages. Circulation. 4 juill 2017;136(1):83-97.

38. Wang L, Cheng J, Hua Z, Liu M, Xu H, Ma Y, et al. α-melanocyte stimulating hormone (α-MSH) promotes osteoblast differentiation of MC3T3-E1 cells. Eur J Pharmacol. 5 févr 2019;844:1-8.

« Par délibération de son Conseil en date du 10 Novembre 1972, l'Université n'entend donner aucune approbation ni improbation aux opinions émises dans les thèses ou mémoires. Ces opinions doivent être considérées comme propres à leurs auteurs ».

VU, le Président de Thèse

VU, le Doyen de la Faculté

VU et permis d'imprimer
en référence à la délibération
du Conseil d'Université
en date du 14 Décembre 1973

Pour le Président
de l'Université de CAEN et P.O

Le Doyen

ANNEE DE SOUTENANCE : 2020

NOM ET PRENOM DE L'AUTEUR : PRIGENT Kevin

TITRE DE LA THESE **: Évaluation d'une thérapeutique préventive chez un modèle de rétrécissement aortique calcifié.**

RESUME DE LA THESE EN FRANÇAIS :

Introduction : La radiothérapie médiastinale est une cause majeure de complications cardiaques incluant le rétrécissement aortique (RA). Cependant il manque de modèle préclinique de RA mimant les lésions radio-induites. De plus le RA est la valvulopathie la plus fréquente. Chez les patients non opérables, sans traitement médical efficace, le pronostic est sombre. Ce projet consiste à évaluer par l'Imagerie et l'Histologie, l'efficacité d'une thérapeutique préventive chez un modèle murin de RA.
Matériels et méthodes : Une irradiation ciblée de la valve aortique (10 ou 20Gy) chez des souris C57/Bl6/J (WT) et ApoE-/- a été réalisé pour développer un modèle de RA. Une fois le modèle mise au point le pyrophosphate inorganique (PPi) a été étudié comme thérapeutique préventive chez des souris ApoE-/- (0 ou 10Gy). Les outils d'évaluation étaient l'échocardiographie et l'imagerie cardiaque par résonance magnétique. Le remodelage cardiaque et valvulaire a été étudié en Histologie utilisant les colorations de von Kossa et Rouge Picro-Sirius.
Résultats : L'irradiation ciblée chez la souris ApoE-/- a démontré le développement d'un RA. Ce RA était caractérisé par une augmentation des vélocités, des gradients trans-valvulaires et l'augmentation de la minéralisation en von Kossa. Le PPi a permis d'annuler complètement les effets observés de la radiothérapie et de démontrer la reproductibilité du modèle chez les souris ApoE-/- non traités.
Conclusion : L'irradiation ciblée sur la valve aortique a permis le développement d'un RA chez la souris ApoE-/-. Basé sur l'Imagerie et l'Histologie, le PPi apparait être un traitement efficace dans ce modèle.

MOTS CLES : Rétrécissement aortique, Radiothérapie, Minéralisation, Imagerie par résonnance magnétique

TITRE DE LA THESE EN ANGLAIS**: Evaluation of a preventive therapy in a model of calcified aortic stenosis.**

RESUME DE LA THESE EN ANGLAIS :

Introduction: Mediastinal radiotherapy is a major cause of cardiac complications including aortic stenosis (AS). However, there is a lack of a preclinical model of AS mimicking radiation-induced lesions. In addition, AS is the most frequent valvular disease. In inoperable patients without effective medical treatment, the prognosis is poor. This project consists in evaluating by Imaging and Histology, the effectiveness of a preventive therapy in a mouse model of AS.
Materials and methods: Targeted irradiation of the aortic valve (10 or 20Gy) in C57 / Bl6 / J (WT) and ApoE - / - mice was carried out to develop an AS model. Once the model had been developed, inorganic pyrophosphate (PPi) was studied as a preventive therapy in ApoE - / - (0 or 10Gy) mice. The assessment tools were echocardiography and cardiac magnetic resonance imaging. Cardiac and valve remodeling was studied in Histology using von Kossa and Rouge Picro-Sirius stains.
Results: Targeted irradiation in ApoE - / - mice demonstrated the development of AS. This AS was characterized by increased velocities, trans-valvular gradients and increased mineralization in von Kossa. The PPi made it possible to completely cancel the observed effects of radiotherapy and to demonstrate the reproducibility of the model in untreated ApoE - / - mice.
Conclusion: Targeted irradiation on the aortic valve allowed the development of an AS in ApoE - / - mice. Based on Imaging and Histology, PPi appears to be an effective treatment in this model.

KEY WORDS: Aortic stenosis, Radiation therapy, Mineralization, Magnetic Resonance Imaging